A review of AVO analysis

Hongbo Zhang and R. James Brown

ABSTRACT

It is usually true that, in looking into the future, people can benefit by reviewing the accomplishments of the past. In this paper, we review many of the milestones in the development of AVO methodology concerning the principles of AVO analysis, the methods of seismic data processing for AVO analysis, the applications of AVO and the techniques in AVO analysis. We have tried to cover the critical formulae and the most current technologies in AVO analysis, including multicomponent and converted-wave AVO, though we make no claims that the review is exhaustive.

INTRODUCTION

The variation of reflection and transmission coefficients with angle of incidence (AVA) (and corresponding increasing offset) is often referred to as offset-dependent reflectivity and is the fundamental basis for amplitude-versus-offset (AVO) analysis. There are two kinds of AVO phenomena according to the types of seismic data. One is P-wave AVO and the other is multicomponent AVO corresponding to single-component P-wave seismic data and multicomponent seismic data, respectively.

Today, AVO analysis is widely used in hydrocarbon detection, lithology identification, and fluid parameter analysis, due to the fact that seismic amplitudes at the boundaries are affected by the variations of the physical properties just above and just below the boundaries.

In recent years, a growing number of theories and techniques in seismic data acquisition, processing, and seismic data interpretation have been developed, updated, and employed. AVO analysis in theory and practice is becoming increasingly attractive.

PRINCIPLES

In exploration geophysics, we rarely deal with simple isolated interfaces. However, we must begin our understanding of offset-dependent reflectivity with the partitioning of energy at just such an interface (Castagna and Backus, 1993). In Figure 1, the angles for incident, reflected and transmitted rays synchronous at the boundary are related according to Snell's law by:

$$p = \frac{\sin\theta_1}{V_{P1}} = \frac{\sin\theta_2}{V_{P2}} = \frac{\sin\phi_1}{V_{S1}} = \frac{\sin\phi_2}{V_{S2}} \tag{1}$$

where V_{P1} = P-wave velocity in medium 1, V_{P2} = P-wave velocity in medium 2; V_{S1} = S-wave velocity in medium 1; V_{S2} = S-wave velocity in medium 2; θ_1 = incident P-wave angle, θ_2 = transmitted P-wave angle, ϕ_1 = reflected S-wave angle, ϕ_2 = transmitted S-wave angle, and p is the ray parameter.

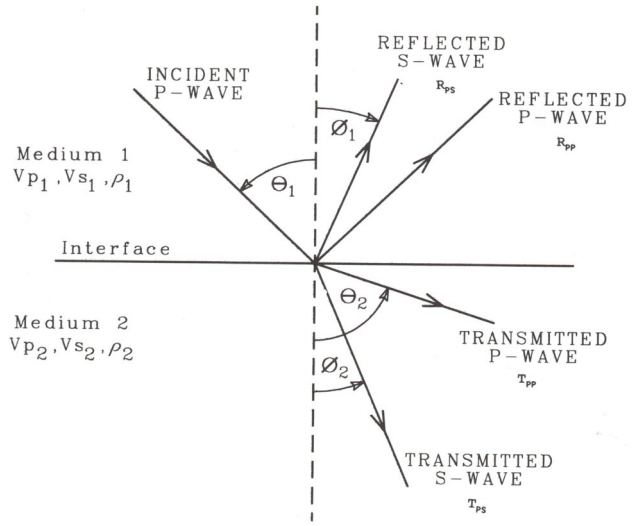

FIG. 1. Reflection and transmission at an interface between two infinite elastic half-spaces for an incident P-wave (Castagna and Backus, 1993)

Knott (1899) and Zoeppritz (1919) invoked continuity of displacement and stress at the reflecting interface as boundary conditions to solve for the reflection and transmission coefficients as functions of incident angle and the elastic properties of the media (densities, bulk and shear moduli), though the resulting Knott and Zoeppritz equations are notoriously complex. Aki and Richards (1980) and Waters (1981) gave an easily solved matrix form

$$Q = P^{-1}R \tag{2}$$

where Q, P, and R are given in Appendix A (Castagna and Backus, 1993).

Koefoed (1955) first pointed out the practical possibilities of using AVO analysis as an indicator of V_P/V_S variations and empirically established five rules, which were later verified by Shuey (1985) for moderate angles of incidence:

"a) When the underlying medium has the greater longitudinal [P-wave] velocity and other relevant properties of the two strata are equal to each other, an increase of Poisson's ratio for the underlying medium causes an increase of the reflection coefficient at the larger angles of incidence.

"b) When, in the above case, Poisson's ratio for the incident medium is increased, the reflection coefficient at the larger angles of incidence is thereby decreased.

"c) When, in the above case, Poisson's ratios for both media are increased and kept equal to each other, the reflection coefficient at the larger angles of incidence is thereby increased.

"d) The effect mentioned in (1) becomes more pronounced as the velocity contrast becomes smaller.

"e) Interchange of the incident and the underlying medium affects the shape of the curves only slightly, at least up to values of the angle of incidence of about 30 degrees."

Bortfeld (1961) linearized the Zoeppritz equations by assuming small changes in layer properties $(\Delta\rho/\rho, \Delta V_P/V_P, \Delta V_S/V_S << 1)$.

This approach was also followed by Richards and Frasier (1976) and Aki and Richards (1980) who derived a form of approximation simply parameterized in terms of the changes in density, P-wave velocity, and S-wave velocity across the interface:

$$R_{PP}(\theta) \approx \frac{1}{2}\left(1 - 4p^2 V_S^2\right)\left(\frac{\Delta\rho}{\rho}\right) + \frac{1}{2\cos^2(\theta)} \cdot \frac{\Delta V_P}{V_P} - 4V_S{}^2\rho^2 \frac{\Delta V_S}{V_S} \tag{3}$$

where $\Delta\rho = \rho_2 - \rho_1$, $\Delta V_P = V_{P2} - V_{P1}$, $\Delta V_S = V_{S2} - V_{S1}$, $\rho = (\rho_2 + \rho_1)/2$, $V_P = (V_{P2} + V_{P1})/2$, $V_S = (V_{S2} + V_{S1})/2$, $\theta = (\theta_1 + \theta_2)/2$ and p is the ray parameter as defined by equation (1). By simplifying the Zoeppritz equations, Shuey (1985) presented another form of the Aki and Richards (1980) approximation,

$$R(\theta) \approx R_0 + \left[A_0 R_0 + \frac{\Delta\sigma}{(1-\sigma)^2} \right] \sin^2\theta + \frac{1}{2}\frac{\Delta V_P}{V_P}\left(\tan^2\theta - \sin^2\theta\right) \tag{4}$$

where R_0 is the normal-incidence P-P reflection coefficient, A_0 is given by:

$$A_0 = B_0 - 2(1 + B_0)\frac{1-2\sigma}{1-\sigma} \tag{5}$$

and

$$B_0 = \frac{\Delta V_P/V_P}{\Delta V_P/V_P + \Delta\rho/\rho} \tag{6}$$

where $\Delta\sigma = \sigma_2 - \sigma_1$ and $\sigma = (\sigma_2 + \sigma_1)/2$.

The quantity A_0, given by equation (5), specifies the variation of $R(\theta)$ in the approximation range $0 < \theta < 30°$ for the case of no contrast in Poisson's ratio. The first term gives the amplitude at normal incidence, the second term characterizes $R(\theta)$ at intermediate angles, and the third term describes the approach to the critical angle.

The coefficients of Shuey's approximation form the basis of various weighted stacking procedures. "Weighted stacking", here also called "Geostack" (Smith and Gidlow, 1987), is a means of reducing prestack information to AVO attribute traces versus time. This is accomplished by calculating the local angle of incidence for each time sample, then performing regression analysis to solve for the first two or all three coefficients of an equation of the kind:

$$R(\theta) \approx A + B\sin^2\theta + C\sin^2\theta\tan^2\theta \tag{7}$$

where A is the "zero-offset" stack, B is commonly referred to as the AVO "slope" or "gradient", and the third term becomes significant in the far-offset stack.

At the same time, the "fluid factor" concept was introduced by Smith and Gidlow (1987) to highlight gas-bearing sandstones. It is discussed further below. Hilterman (1989) derived another convenient approximation:

$$R(\theta) \approx R_0 \cos^2 \theta + 2.25 \Delta\sigma \sin^2 \theta \tag{8}$$

where the definitions of the parameters are the same as above.

Thus, at small angles R_0 dominates the reflection coefficient whereas $\Delta\sigma$ dominates at larger angles. In this way, we can think of a near-offset stack as imaging P-wave impedance contrasts while the far-offset stack images Poisson's-ratio contrasts.

In recent years, converted-wave AVO (C-AVO) has become popular. However, time-domain stacking procedures naturally corrupt all C-AVO effects in assembling the stacked common-conversion-point (CCP) trace. A simple modification to those procedures is employed by Thomsen (1999), so that the necessary information is preserved. The modification involves the construction of flattened CCP gathers, each with a common conversion point, x_c, for all events (all times t_{c0}) and all offsets, s (x_{c0}, x, t_{c0}). It is exactly the time-domain stacking procedure, except that the CCP amplitudes are not added together; instead, the C-AVO behaviour is preserved for analysis.

SEISMIC DATA PROCESSING FOR AVO/AVA ANALYSIS

According to Castagna and Backus (1993), when attempting to select an appropriate data-processing scheme for AVO analysis, the processor must carefully balance two competing objectives: (1) noise suppression and isolation of the reflectivity of the event of interest, and (2) not biasing or otherwise corrupting the reflectivity variation with offset. This tradeoff usually leads to the selection of a basic but robust processing scheme (for example, Ostrander, 1984; Chiburis, 1984) (Table 1).

Amplitude-variation-with-angle (AVA) analysis is preferable to AVO analysis when comparing a deeper target with a shallower one. On the other hand, AVA analysis requires information about velocities and raypaths that is not needed for AVO analysis. In practice, both offset and angle displays may be helpful to the interpreter because each offers a different perspective on the data.

Wapenaar (1999) pointed out a prominent problem concerning AVA, that is, that the fine layering near the Earth's surface causes apparent AVA effects in seismic reflection data (Figure 2). The distinction between reflection- and propagation-related apparent AVA effects is that the reflection of a package of thin layers is accompanied by angle-dependent wavelet interference, whereas propagation through finely layered media causes angle-dependent wavelet dispersion. These are not what we want in the data processing for AVO analysis.

Ostrander (1984):	1. Spherical-divergence correction
	2. Exponential-gain correction
	3. Minimum-phase spiking deconvolution
	4. Velocity analysis
	5. NMO correction
	6. Trace equalization
	7. Horizontal trace summing
Chiburis (1984):	1. Mild *f-k* multiple suppression
	2. Spherical divergence and NMO correction
	3. Whole-trace equalization
	4. Flattening on a consistent reference event
	5. Horizontal trace summing
	6. Peak amplitude picked interactively
	7. Smoothed least-squares curve fitting
	8. Despiking of outliers
	9. Results clipped and smoothed
	10. Curve refitting

Table 1. Examples of processing schemes reported in the literature (Castagna and Backus, 1993).

Wapenaar's solution is as follows: by applying an angle-dependent filter in the imaging step in angle-dependent migration schemes, the reflection-related interference effects can be equalized, though they cannot be removed. The propagation-related dispersion effects can be compensated for in the downward extrapolation process by means of inverse generalized primary propagators (Figure 3).

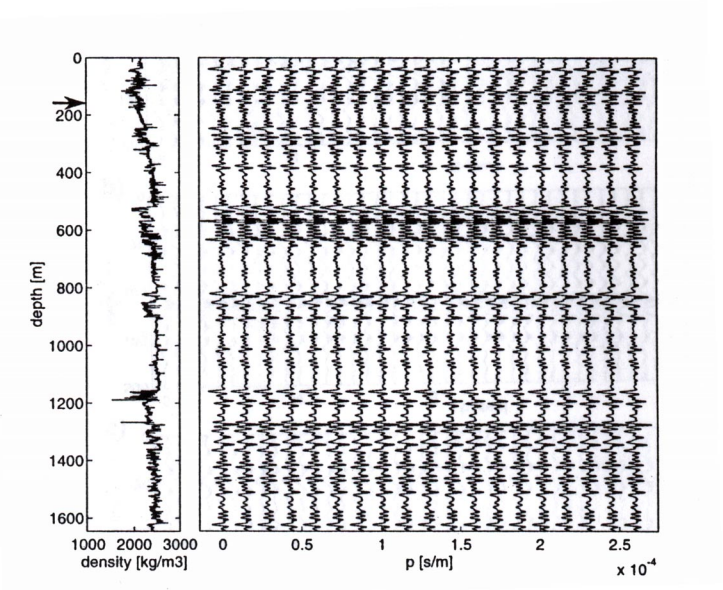

FIG. 2. Reflectivity section obtained with standard 1-D angle-dependent migration. Note the apparent AVA behaviour (Wapenaar et al., 1999).

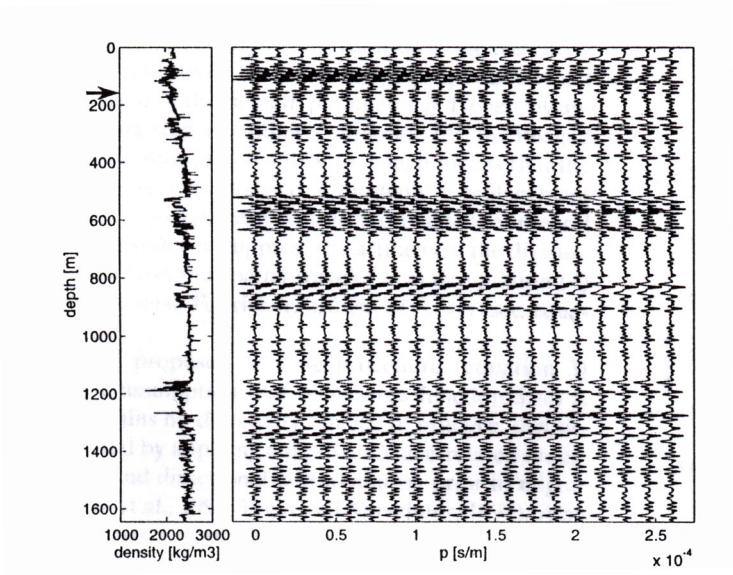

FIG. 3. Reflectivity section obtained with 1-D angle-dependent migration including the modified imaging step. Note that the AVA has been removed (Wapenaar et al., 1999).

An interesting phenomenon was noticed by Carcione (1999). Waves transmitted at the ocean bottom have the characteristic(s) that, for any incidence angle, the attenuation vector is perpendicular to the ocean-bottom interface (assuming water to be a lossless medium). Such waves are called inhomogeneous. The attenuation vector can be written as follows,

$$\alpha \equiv [\mathrm{Im}(s_x), \mathrm{Im}(s_z)]^T \tag{9}$$

where s_x and s_z are the components of the complex slowness vector.

The vector character of this transmitted pulse affects the amplitude-variation-with-offset (AVO) response of deeper reflectors. Carcione also noticed that amplitude and phase differences are significant at supercritical angles. Variations of the attenuation depend on both the anisotropic properties and the inhomogeneity of the wave. His conclusion is that AVO studies in the presence of a highly attenuating ocean bottom (e.g., unconsolidated sediments) should not be based on forward models and processing techniques that assume simplified rheologies or neglect the vector attenuation character of the seismic pulse.

Linear regression is a widely used method in the data processing for AVO analysis. A robust approach to linear regression, the least median squares (Rousseeuw and Leroy, 1987), is proposed by Ferre et al. (1999) for improving the intercept and gradient computation in the presence of noise and outlier contamination. This approach is demonstrated on a real case study, together with the use of quality-control diagnostics, leading to a global improvement of the standard AVO methodology.

A new approach to improving AVO analysis in the presence of dip is demonstrated by Ramos et al. (1999). This approach is called true-amplitude DMO. True-amplitude DMO shares the benefits of reducing the amplitude mix caused by smearing and mispositioning of reflection points. The main advantage of true-amplitude DMO compared to more traditional methods lies in its ability to perform a better compensation of geometrical-spreading losses with offset. The more reliable amplitude obtained upon the application of true-amplitude DMO on a real dataset example including an AVO anomaly, made possible a better estimation of AVO attributes such as AVO gradient and better delineation and enhancement of AVO anomalies (Figure 4).

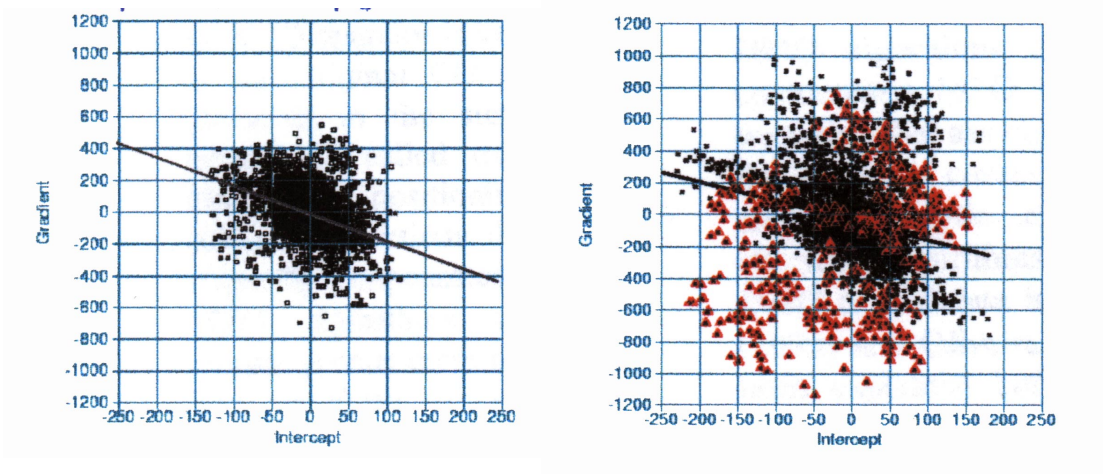

FIG. 4. Crossplot gradient versus intercept for the seismic data processed with *f-k* DMO (left) and true-amplitude DMO (right) (Ramos et al., 1999).

In the *f-k* DMO case, a considerably smaller scatter of the amplitudes around the background trend is observed. This smaller scatter is caused by the poor gradient estimation, particularly for long offsets and dipping events. The crossplot for the true-amplitude DMO case shows a significantly larger scatter and better separation of the anomalous values in the first and third quadrants, due to more accurate geometrical-spreading compensation of amplitudes at far offsets (Ramos et al., 1999).

APPLICATION OF AVO DATA

Gas detection

By far, gas-sand detection is the most promising application of AVO analysis. It is hoped that the characteristically low V_P/V_S ratio of gas sands should allow their differentiation from other low-impedance layers, such as coals and porous brine sands (Castagna et al., 1993). Rutherford and Williams (1989) defined three distinct classes of gas-sand AVO anomalies. Their Class 1 occurs when the normal-incidence P-wave reflection coefficient is strongly positive and shows a strong amplitude decrease with offset and a possible phase change at far offset (Figure 5).

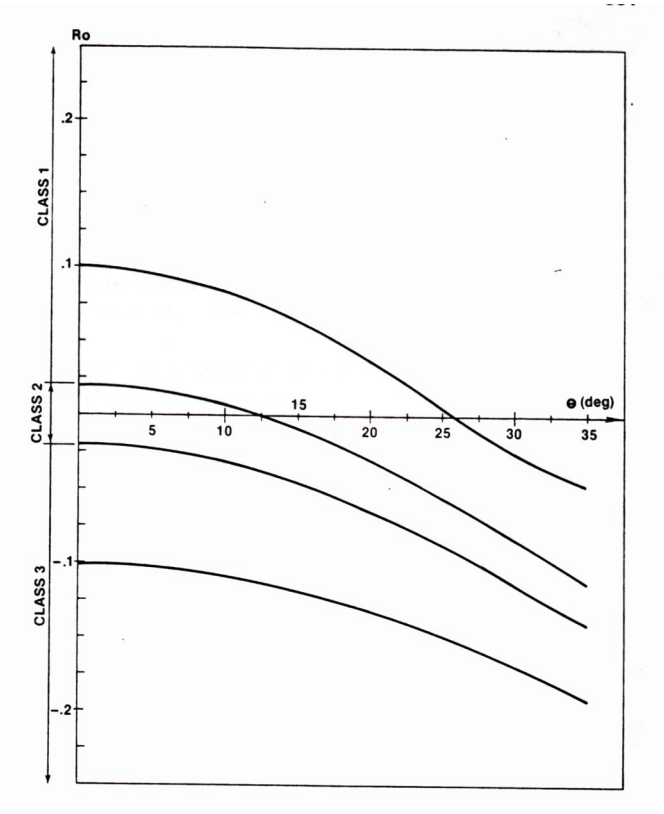

FIG. 5. Zoeppritz P-wave reflection coefficients for a shale/gas-sand interface for a range of R_0 values. The Poisson's ratio and density of the shale were assumed to be 0.38 and 2.4 g/cm^3, respectively. The Poisson's ratio and density of the gas sand were assumed to be 0.15 and 2.0 g/cm^3, respectively (Rutherford and Williams, 1989).

Class 2, for small P-wave reflection coefficients, shows a very large percent change in AVO. In this situation, if the normal-incidence reflection coefficient is slightly positive, a phase change at near or moderate offsets will occur. Class 3 anomalies (Rutherford and Williams, 1989) have a large negative normal-incidence reflection coefficient, which becomes more negative as offset increases (these are classical bright spots). A simple rule of thumb that generally applies to shale over gas-sand reflections is that the reflection coefficient becomes more negative with increasing offset (Castagna and Backus, 1993).

But on the principles of AVO crossplotting, Castagna and Swan (1997) suggest that hydrocarbon-bearing sands overlain by shale should be classified according to their location in the A-B plane, rather than by their normal-incidence reflection coefficient alone. Class I sands (Castagna et al., 1997) are of higher impedance than the overlying unit. They occur in quadrant IV of the A-B plane. The normal incidence reflection coefficient is positive while the AVO gradient is negative. And the reflection coefficient decreases with increasing offset. Class II sands (Castagna et al., 1997) have about the same impedance as the overlying unit. They exhibit highly variable AVO behaviour and may occur in quadrants II, III, or IV of the A-B plane. Class III sands (Castagna and Swan, 1997) here are of lower impedance than the overlying unit and are frequently "bright." (Figure 6).

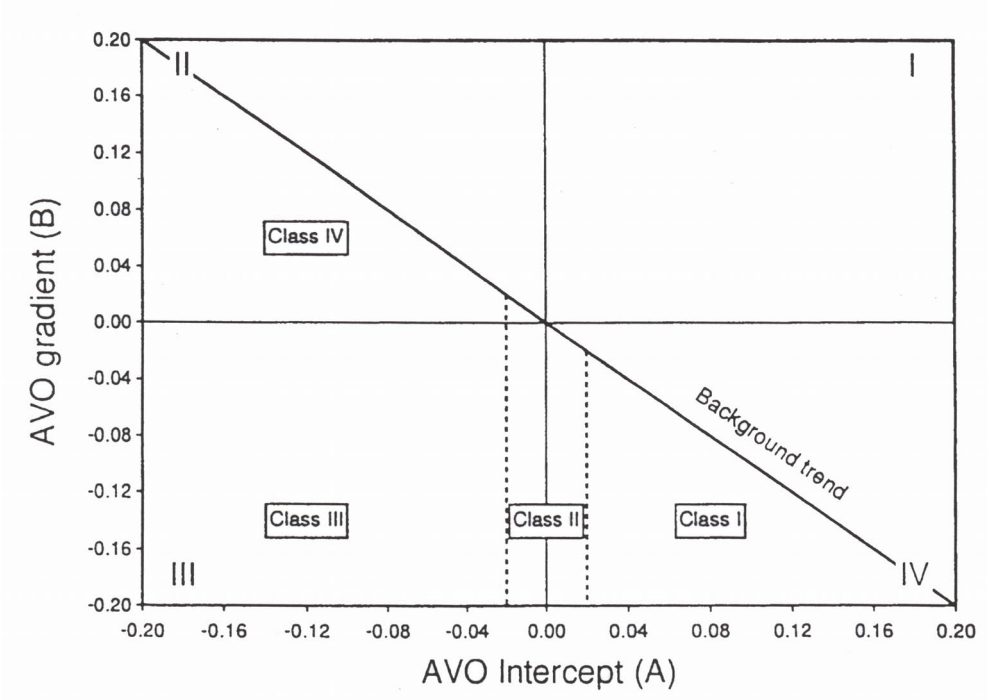

FIG. 6. This newer classification is identical to that of Rutherford and Williams (1989) for Class I (high-impedance-contrast) and Class II (low-impedance-contrast) sands. However, it differs in that Class III (low-impedance-contrast) is subdivided into two classes, III and IV. The Class IV sands are highly significant in that they exhibit AVO behaviour contrary to established rules of thumb and occur in many basins throughout the world, including the Gulf of Mexico (Castagna and Swan, 1997). (Numbers in the corners are quadrant numbers.)

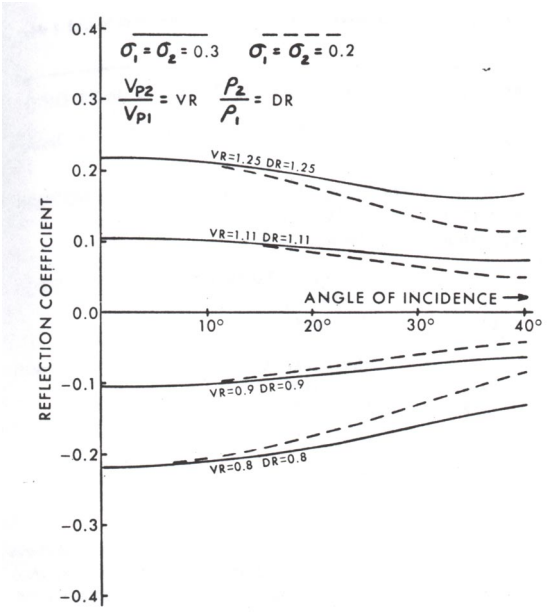

FIG. 7. P-wave reflection coefficient versus angle of incidence for constant Poisson's ratios of 0.2 and 0.3 (Ostrander, 1984).

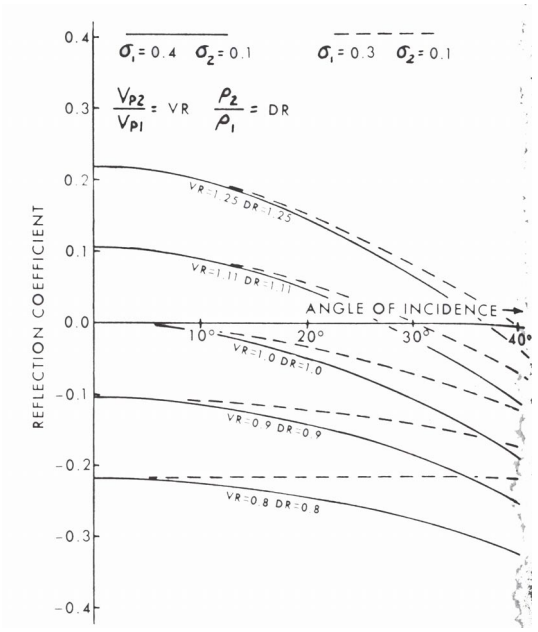

FIG. 8. P-wave reflection coefficient versus angle of incidence for a reduction in Poisson's ratios across an interface (Ostrander, 1984).

The most famous story in the detection of gas in sandstone reservoirs using AVO analysis is that of Fatti et al. (1994). They employed a technique called Geostack (Smith and Gidlow, 1987). The fluid factor (Smith and Gidlow, 1987) here is defined as:

$$\Delta F = R_{PP} - 1.16\frac{W}{V}R_{SS} \tag{10}$$

where R_{PP} = zero-offset P-P reflection coefficient, W = average S-wave velocity, V = average P-wave velocity, R_{SS} = zero-offset S-wave reflection coefficient.

The success of the ΔF traces in indicating the presence of gas depends on the amount of separation on the crossplot of W versus V for gas sandstones, on the one hand, and water sandstones and shales on the other hand (Figure 9).

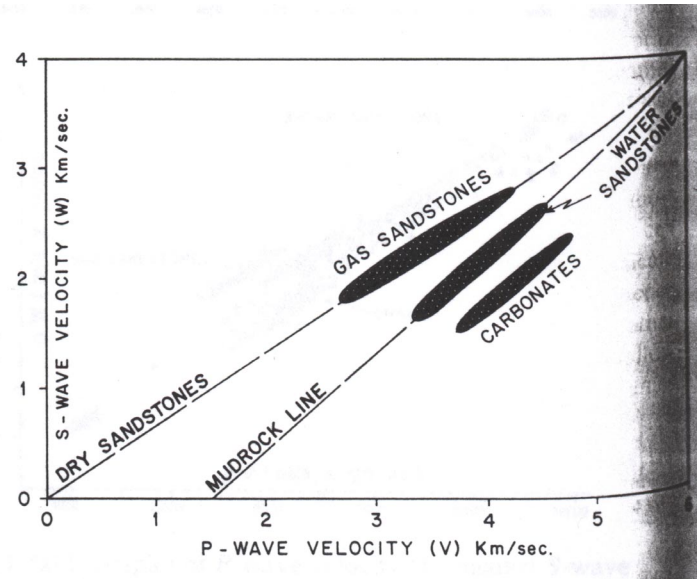

FIG. 9. Diagrammatic crossplot of P-wave velocity against S-wave velocity (Fatti et al., 1994; after Castagna et al., 1985).

In order to improve the crossplot analysis, Ross and Sparlin (2000) employed visualization techniques. They found that the interpretation of the AVO crossplot and examination of the crossplot data with 3-D visualization techniques permit rapid identification of the background trend and anomalies using large data volumes (Figure 10).

With the emergence of converted-wave methods, Garotta and Granger (1987) carried out research on compressional and converted-wave acquisition and processing in a sand/shale environment above a carbonate layer providing a good reflection marker. They compared the responses of the P mode and of the P-SV mode with respect to the following points: amplitude versus incidence angle on the gas sand; amplitude decay through the gas-sand; and frequency spectra. The theoretical responses derived from a depth model by means of the Zoeppritz equations are compared with actual data, showing reasonable agreement (Figures 11 to 15).

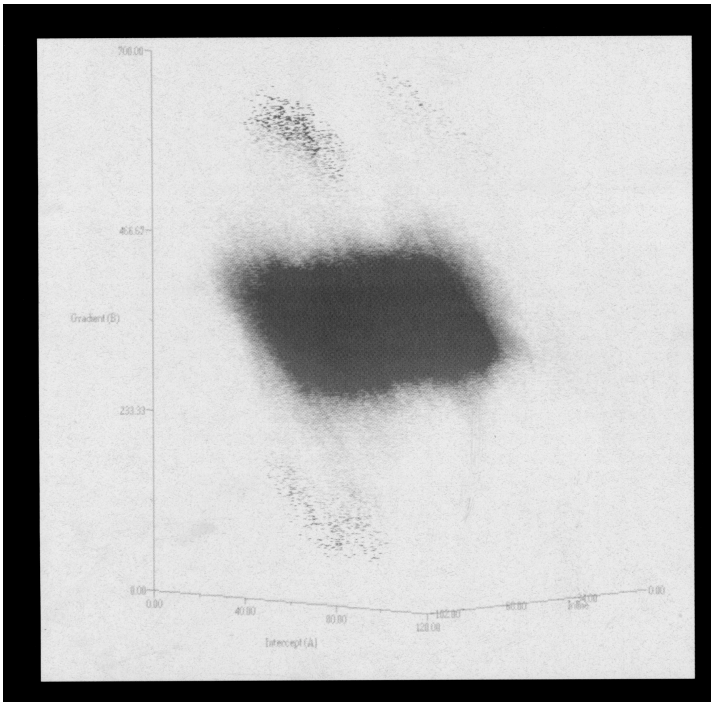

FIG. 10. The dark cloud at the centre is interpreted as giving the correct values of intercept, *A* (horizontal axis), and gradient, *B* (vertical axis).

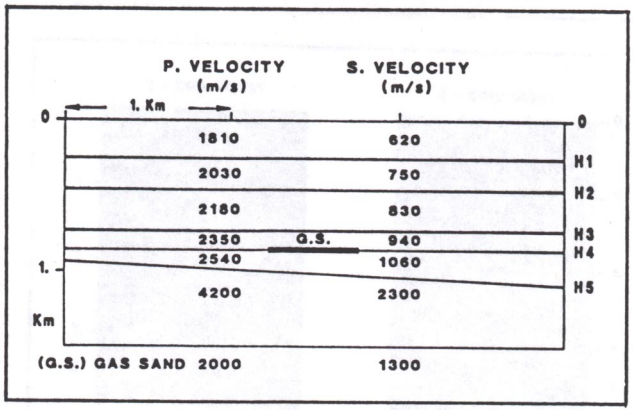

FIG. 11. Depth model (Garotta and Granger, 1987).

Another use of AVO analysis in gas detection is the use of Biot-type three-phase theory by Carcione and Tinivella (2000). Bottom-simulating reflectors (BSRs) on seismic profiles are interpreted as representing the seismic signature of the base of gas-hydrate formation. A free-gas zone may be present just below the BSR (Carcione and Tinivella, 2000). Their research assumes that the BSR is caused solely by an interface separating cemented gas-hydrate- and free-gas-bearing sediments. They conclude that low and high concentrations of hydrate can be distinguished since they give positive and negative anomalies, respectively, and that the P-to-S reflection coefficient is a good indicator of high amounts of free gas and gas hydrate (Figures 16 and 17).

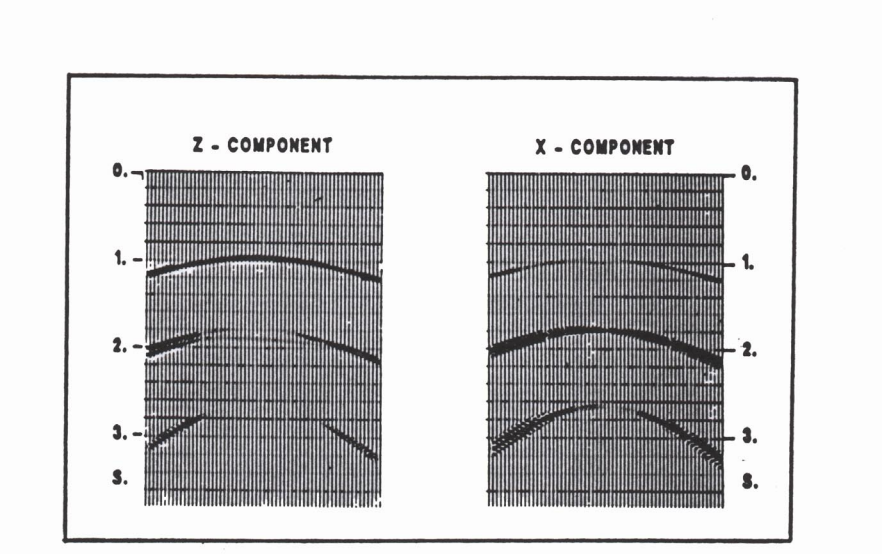

FIG. 12. Synthetic data (cf. Figure 11) via Zoeppritz equations (Garotta and Granger, 1987).

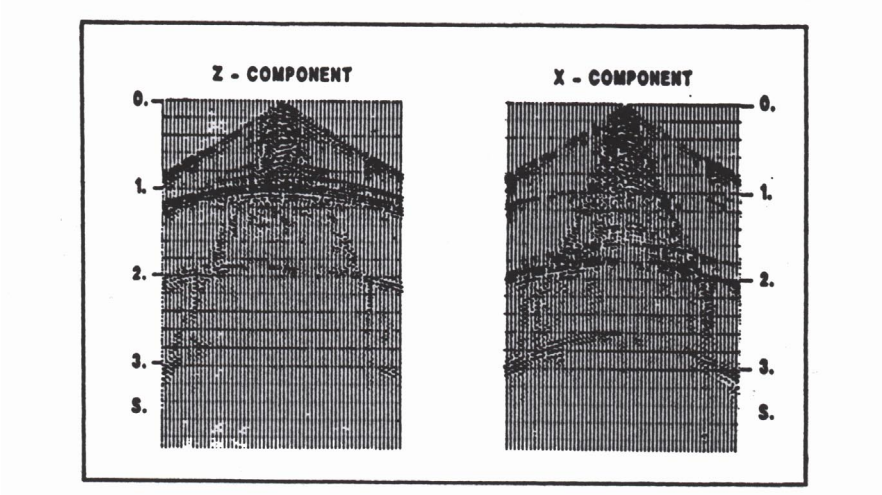

FIG. 13. Actual data showing mainly H4 (cf. Figures 11 and 12) (Garotta and Granger, 1987).

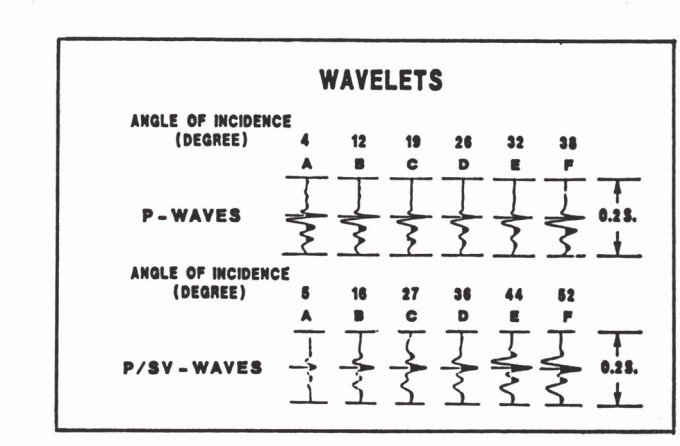

FIG. 14. P and P-SV wavelets on horizon H4 versus angle of incidence; the P-SV wave has a more obvious AVO effect (Garotta and Granger, 1987).

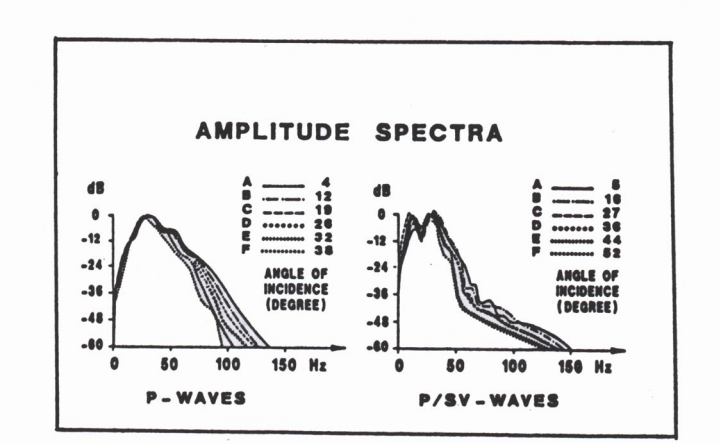

FIG. 15. P and P-SV wave amplitude spectra; the P-SV waves have broader spectra (Garotta and Granger, 1987).

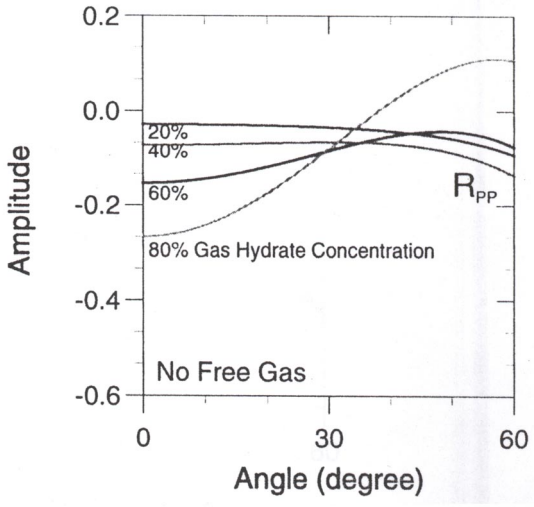

FIG. 16. P-P reflection coefficient versus incidence angle (Carcione and Tinivella, 2000).

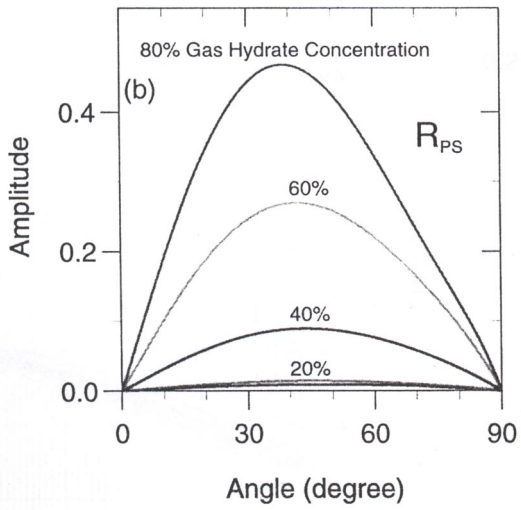

FIG. 17. P-S reflection coefficients versus incidence angle (Carcione and Tinivella, 2000).

In regional seismic exploration, a challenge often faced by geophysicists is to determine AVO applicability and effectiveness in the region. What is often lacking in the decision-making process is a quantitative measure of the errors caused by wave propagation and inversion procedures. Swan (1991) discusses in general terms five sources of error for AVO intercept/slope estimates, including NMO stretch and thin-bed tuning. Dong (1999) addresses the problems related to the detectability of AVO in the presence of stretching and thin-bed tuning artifacts on the basis of Swan's (1991) work and his own (Dong, 1996). Two simple criteria have been obtained to quantify the minimum V_P/V_S change needed for an AVO event to survive the contamination caused by the effects of migration stretch and thin-bed tuning. In the case of pure stretching, the detectability condition is given by Dong (1999) as:

$$\frac{|\delta\gamma|}{\gamma} > 0.15\gamma^2 |A|_{\max} \tag{11}$$

where $|A|_{\max}$ is the maximum intercept value for background reflectors that are close to the AVO reflector, $\gamma = V_P/V_S$.

In the case of tuning plus stretching, the requirement of the detectability condition is much more stringent and involves the thin-bed parameter. The detectability condition in this case (Dong, 1999) is:

$$\frac{|\delta\gamma|}{\gamma} > 0.41\gamma^2\xi|A|_{thin} \tag{12}$$

where ξ is the thin-bed parameter and $\xi = 2\pi h/\lambda_0$, $\lambda_0 = V_{above}/f_0$.

Lithology identification

The petrophysical "signal" for AVO lithology analysis is the lithology dependence of V_P/V_S . Castagna et al. (1985) concluded that shear-wave velocity is nearly linearly related to compressional-wave velocity for both water-saturated and dry siliciclastic sedimentary rocks (Figure 18).

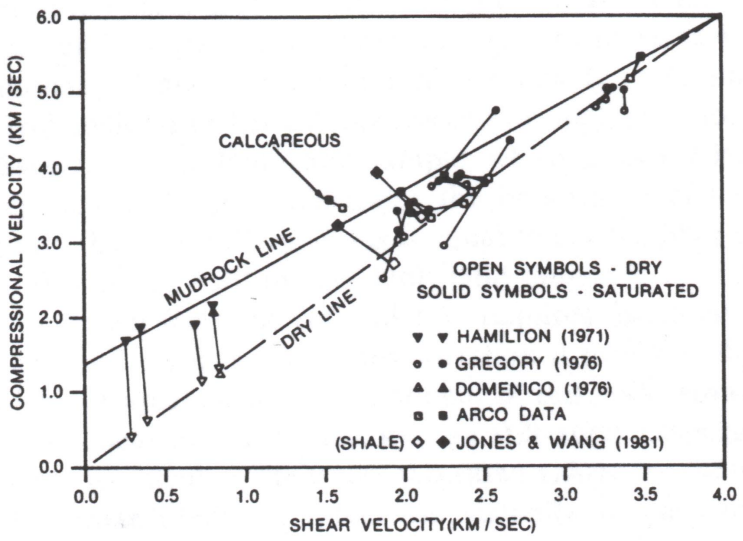

FIG. 18. Ultrasonic laboratory data for various sandstones under both dry and saturated conditions. Dry (open symbols) and saturated (solid symbols) data are plotted for the same effective pressure conditions and joined by tie lines (Castagna et al., 1985).

Then Hilterman (1990) summarized the two steps in an AVO analysis: (1) the extraction of the rock properties from the CDP gather, and (2) relation of lithology to the extracted rock properties. With regard to the first step, Shuey (1985) introduced a classic expression for the AVO seismic response in terms of the rock properties. An approximation of Shuey's reflection coefficient equation is:

$$R(\theta) \approx R_0 \cos^2(\theta) + 2.25\Delta\sigma \sin^2(\theta) \tag{13}$$

where R_0 is the normal-incidence reflection coefficient and $\Delta\sigma$ is the change in Poisson's ratio from the upper medium to the lower.

Verm and Hilterman (1995) found that if the S-wave to P-wave velocity ratio is approximately 0.5 and the terms that are insignificant below 30° are dropped, then Shuey's (1985) AVO equation can be reduced to two terms, a normal-incidence reflectivity term, NI, and a far-offset reflectivity term, PR. So:

$$R(\theta) \approx NI \cos^2(\theta) + PR \sin^2(\theta) \tag{14}$$

with NI and PR defined by:

$$NI = \frac{\alpha_2\rho_2 - \alpha_1\rho_1}{\alpha_2\rho_2 + \alpha_1\rho_1} = R_0, \text{ and } PR = \frac{\sigma_2 - \sigma_1}{(1-\sigma_{avg})^2}. \tag{15}$$

In this way, the single-parameter analysis (NI) is extended to a two-parameter analysis (NI and PR). By colour-coding the NI-PR matrix, a more effective discriminator of lithologies develops because the separation of reflection clusters increases (Figure 19).

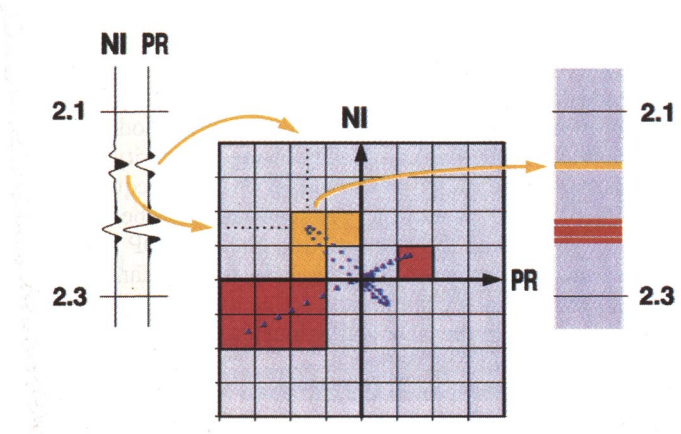

FIG. 19. Colour-coding (here in greyscale) a matrix table to transform the two attribute traces on the left into the single attribute trace on the right (Verm and Hilterman, 1995).

Later, Goodway et al. (1997) introduced, (1) an improved petrophysical discrimination of rock properties using $\lambda\rho$ and $\mu\rho$ over conventional V_P/V_S analysis; (2) greater physical insight by isolating reservoir rock properties for pore fluid and lithology into the moduli or Lamé-parameter terms of their seismic responses; (3) easier AVO crossplot thresholding for a more sensitive "$\lambda\rho$, $\mu\rho$ fluid factor" type stack; (4) a new $\lambda\rho$ stack showing gas zones without interpretive thresholding or fluid-factor choices.

Foster and Keys (1999) further investigated the effects of changes in rock properties on AVO responses. Their exact expression for intercept and slope:

$$B = (1-8\gamma^2)A - 4\gamma\Delta\gamma(1-\Delta\gamma) + (1-2\gamma)O(A^2) \qquad (16)$$

shows that the fluid-line trend has the least scatter when $V_P/V_S = 2$, and base-of-sand reflections are more prominent than top-of-sand reflections (Figure 20).

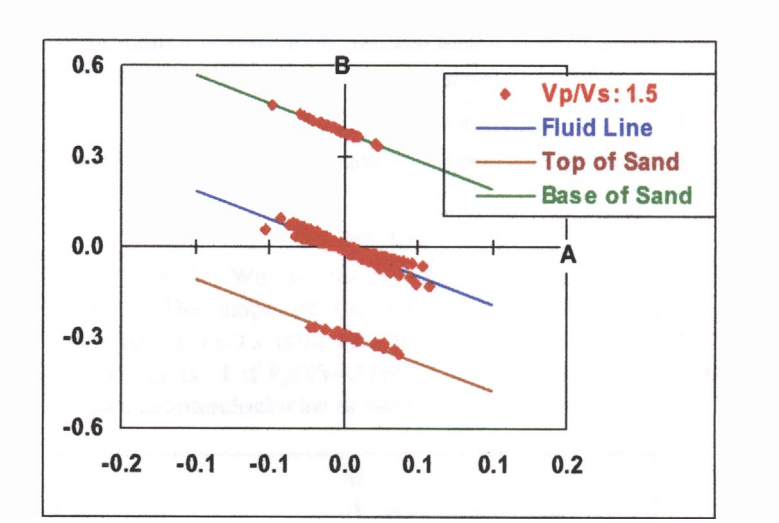

FIG. 20. Predicted trends from equation (16) versus slope (*B*) and intercept values (*A*) (Foster and Keys, 1999).

The fluid line is important because reflections from wet sands and shales, which have little contrast in V_P/V_S, tend to fall on the fluid-line trend; reflections from hydrocarbon-bearing sands do not. Gray et al. (1999) derived two new AVO equations that related the change in seismic amplitude with offset to the fundamental elastic rock properties of shear modulus, μ, density, and either bulk modulus or first Lamé modulus, λ. The reflectivities of the fundamental rock properties derived by these equations correlate well with the values derived directly from logs.

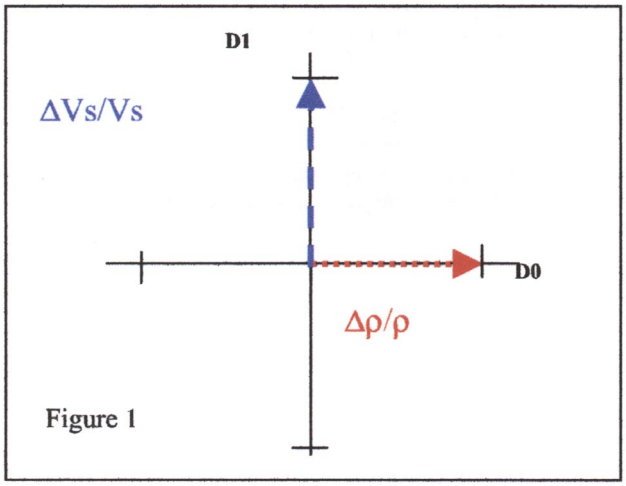

FIG. 21. P-S attribute crossplot displacements associated with the density and V_S for the case of a D0 versus D1 crossplot (Kelly and Ford, 2000b)

Kelly and Ford (2000a) found the interpretation of AVO attribute crossplots can be simplified by utilizing the fact that observed displacements from the background trend are the result of summing the displacements associated with the individual rock property contrasts. Displacements provide information not only about how rock properties change across an interface but about how they change spatially and temporally (Kelly and Ford, 2000b) (Figures 21 and 22).

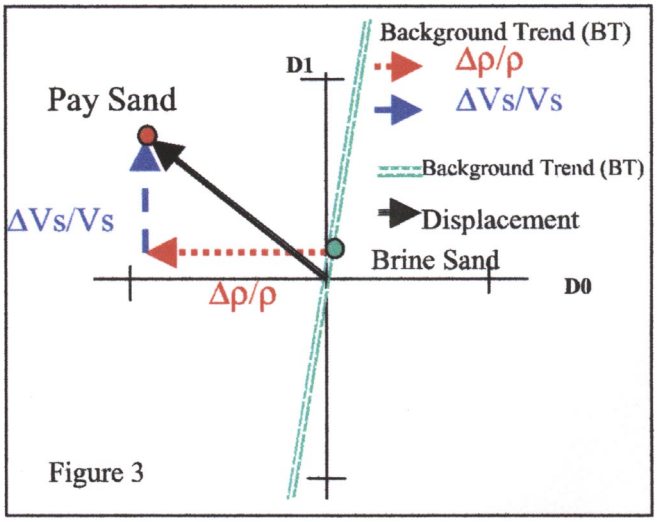

FIG. 22. Shale/brine sand displacement and the additional displacements due to hydrocarbon substitution. Summing these displacements results in the shale/gas-sand displacement. The background trend (BT) on which the shale/brine sand falls is also shown (Kelly and Ford, 2000b).

Anisotropy

The expressions for P-P reflection coefficients at interfaces where at least one medium is anisotropic are very complicated; however, empirical and analytical studies have shown that anisotropy can significantly affect AVO analysis (Wright, 1987; Banik, 1987; Mallick and Frazer, 1991; Kim et al., 1993; Thomsen, 1993; Blangy, 1994). Rüger (1997, 1998) has derived approximations to the analytical solutions that give intuition and insight into the influence of transverse isotropy, both VTI and HTI, on AVO signatures. Rüger shows that the offset variation of the P-wave reflection coefficient is quite sensitive to even relatively weak anisotropy and, in the HTI case, is also quite sensitive to azimuth. He also demonstrates that his approximations – analogous to those of Aki and Richards (1980) – give accurate results even for rather large angles of incidence.

INVERSION

Seismic inversion involves the computation of an Earth model that is compatible with observed seismic data on the basis of an assumed functional relationship between the Earth model and the noise-free data. But Mahob et al. (1999) illustrated the potential pitfalls of linearized AVO inversion when a reliable starting model is not available.

Acoustic-impedance inversion is a commonly used inversion method. Malkin et al. (1999) proposed a method using eigenvector-basis expansion. This method correctly treats the convolutional model for short-trace fragments and is most convenient for incorporating geological constraints. They also demonstrated that AVO-attribute amplitude inversion can add to the conventional acoustic-impedance section new important information valuable for solving oil-and-gas prospecting problems.

To efficiently invert seismic amplitudes for elastic parameters, a pseudoquartic approximation to the Zoeppritz equations was derived by Wang (1999) to calculate P-P reflection and transmission coefficients as a function of the ray parameter. Therefore, one can potentially estimate not only two (in conventional AVO) but three key parameters from an amplitude inversion.

Traditionally, AVO analysis is mainly performed on P-wave data because of the poor quality of S-wave data. But recent developments in ocean-bottom-seismic (OBS) technology make it possible to acquire high-quality S-wave data in the marine environment. Jin (1999) presents a real data example using P and S waves jointly in AVO analysis. Combining P- and S-wave data, the multi-parameter inversion improves reservoir descriptions, especially for fluid-contact detection and pore-fill discrimination.

In the same year, Larsen et al. (1999) developed a method to simultaneously invert P-P and P-S prestack seismic data to extract estimates of compressional and shear impedance values. Initial results show that there is a general improvement using both types of data, that events appear more coherent, and that signal-to-noise appears to have increased. Ronen (2000) further proposes a method of multicomponent AVO inversion that may yield more information from multicomponent data than conventional state-of-the-art methods of separate P-P and P-S AVO inversion. This idea is to use the AVO of both P-P and P-S data simultaneously to estimate acoustic and elastic impedance contrasts, density contrasts and Lamé parameters. Then one inverts the contrasts to estimate the parameters themselves. An example of this application is shown in Figure 23.

Kelly et al. (2000) demonstrated another converted-wave inversion method called P-P and P-S angle-stack inversion to be one of the simplest and most effective tools for determining qualitative AVO signatures, though they do not uniquely identify zones of fully saturated pay with good reservoir quality. But relationships can be constructed between angle stack amplitudes and the rock-property contrasts that produce the reflections. The relationships can be inverted, resulting in predictions of rock-property contrasts in terms of a collection of angle stacks. Rock-property contrasts are simpler to interpret and can be compared directly with well logs. They provide greater sensitivity to fluid type, porosity, saturation and frame characteristics (Kelly et al., 2000) (Figure 24).

The defining of seismic velocity and density also takes advantage of converted-wave seismic data. By using two wave modes (P and S) instead of only one (P), it is possible to derive the densities and compressional and shear velocities in a more robust way once the V_P/V_S relationship is established (Garotta et al., 2000).

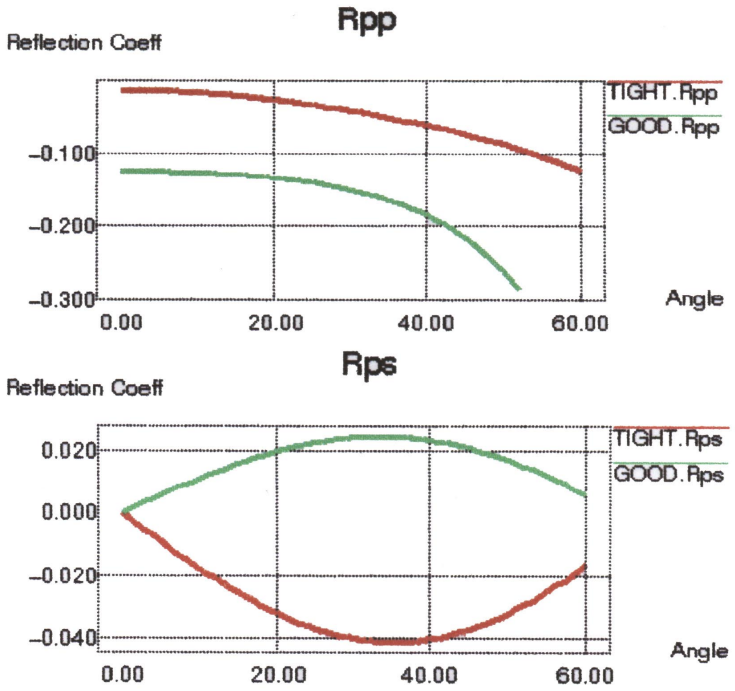

FIG. 23. P-P reflection (top) and P-S conversion coefficients (bottom) versus angle for 'tight' and 'good' reservoir scenarios (Ronen et al., 2000).

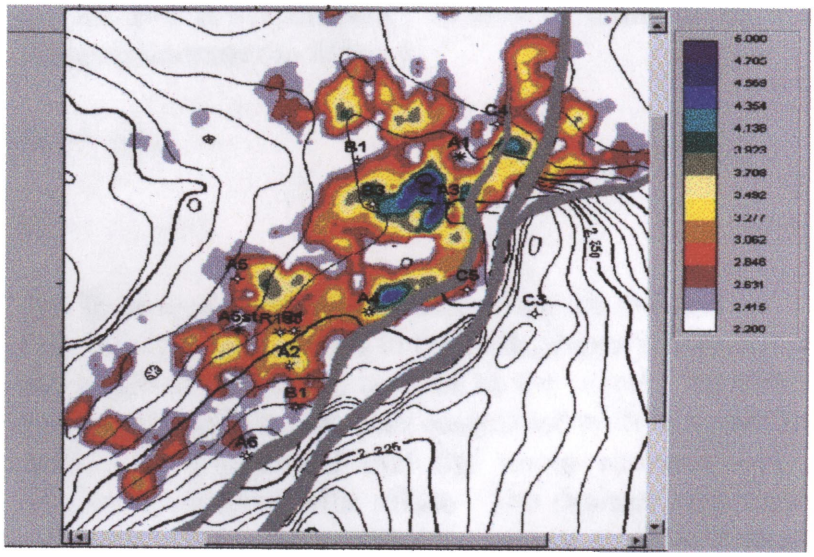

FIG. 24. Density-contrast map derived from angle-stack data. The result agrees with the well data (Kelly et al., 2000).

Recently, Jin et al. (2000) applied AVO inversion to an OBS data set from the North Sea and illustrated the practical use of the S-wave AVO inversion by the combined use of S-wave velocity and density to seismic reservoir characterization, especially for fluid contact detection and changes in pore fluids. Jin and Michelena (2000) developed a prestack seismic-inversion technique that performs most tasks of transforming the recorded data to rock physical properties. Application to the

Mahogany dataset (Figure 25) shows that this inversion is capable of extracting some critical elastic parameters from multicomponent data in a structurally complex area.

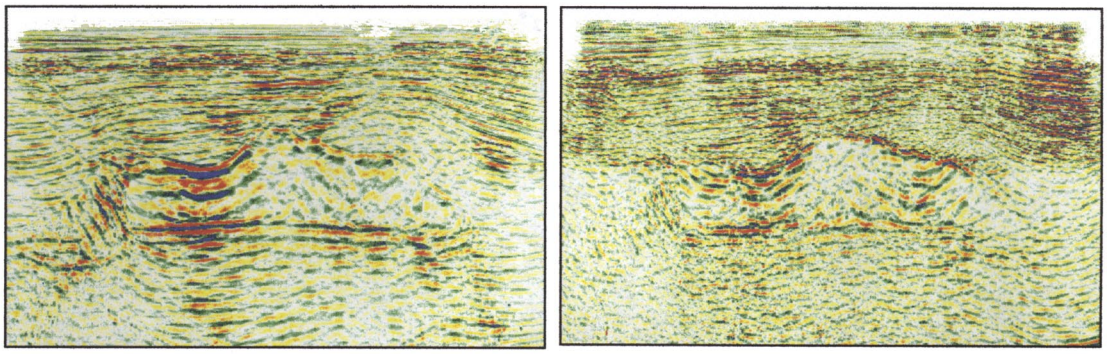

FIG. 25. P-impedance contrast map (left) and S-impedance contrast map (right) (Jin and Michelena, 2000).

CONCLUSIONS

We have reviewed approximately 50 research papers on AVO analysis, which include the principles of AVO, seismic data processing for AVO analysis, interpretation of AVO data, and inversion for AVO analysis. This review is not intended to be exhaustive but should give the reader a good introduction to the development of the theories and techniques of AVO analysis and many of the most recent accomplishments in AVO applications.

The main trend in the AVO development is shifting from more theoretical studies to more applications, from P-wave seismic data to multicomponent seismic data. This trend results in successful solutions to more and more challenging problems encountered by scientists in petroleum exploration as well as mineral exploration.

ACKNOWLEDGEMENTS

We would like to thank the sponsors of the CREWES Project for their continued support, and Gary Margrave and Larry Lines for their excellent suggestions and encouragement.

REFERENCES

Aki, K., and Richards, P.G., 1980, Quantitative seismology: Theory and methods: W. H. Freeman and Co.

Banik, N.C., 1987, An effective anisotropic parameter in transversely isotropic media: Geophysics, **52**, 1654-1664.

Blangy, J.P., 1994, AVO in transversely isotropic media: Geophysics, **59**, 775-781.

Bortfeld, R., 1961, Approximation to the reflection and transmission coefficients of plane longitudinal and transverse waves: Geophys. Prosp., **9**, 485-503.

Carcione, J.M., 1999, Effects of vector attenuation on AVO of offshore reflections: Geophysics, **64**, 815-819.

Carcione, J.M. and Tinivella, U., 2000, Bottom-simulating reflectors: seismic velocities and AVO effects: Geophysics, **65**, 54-67.

Castagna, J.P. and Backus, M.M., 1993, AVO analysis-tutorial and review, *in* Castagna, J. and Backus, M.M., eds, Offset-dependent reflectivity – Theory and practice of AVO analysis: Soc. Expl. Geophys., 3-37.

Castagna, J.P. and Swan, H.W., 1997, Principles of AVO crossplotting: The Leading Edge, **16**, 337-342.

Castagna, J.P., Batzle, M.L., and Eastwood, R.L., 1985, Relationships between compressional-wave and shear-wave velocities in clastic silicate rocks: Geophysics, **50**, 571-581.

Chiburis, E.F., 1984, Analysis of amplitude versus offset to detect gas-oil contacts in Arabia Gulf: 54th Ann. Internat. Mtg., Soc. Expl. Geophys., Expanded Abstracts, 669-670.

Dong, W., 1996, Fluid line distortion due to migration stretch: 61st Ann. Internat. Mtg., Soc. Expl. Geophys., Expanded Abstracts, 1345-1348.

Dong, W., 1999, AVO detectability against tuning and stretching artifacts: Geophysics, **64**, 494-503.

Fatti, J.L., Smith, G.C., Vail, P.J., Strauss, P.J., and Levitt, P.R., 1994, Detection of gas in sandstone reservoirs using AVO analysis: a 3-D seismic case history using the Geostack technique: Geophysics, **59**, 1362-1376.

Ferre, A., Fournier, F., and Lucel, N., 1999, Improving AVO attributes with robust regression and quality control: 69th Ann. Internat. Mtg., Soc. Expl. Geophys., Expanded Abstracts, 848-851.

Foster, D.J., and Keys, R.G., 1999, Interpreting AVO responses: 69th Ann. Internat. Mtg., Soc. Expl. Geophys., Expanded Abstracts, 748-751.

Garotta, R.J. and Granger, P.Y., 1987, Comparison of responses of compressional and converted waves on a gas sand: 57th Ann. Internat. Mtg., Soc. Expl. Geophys., Expanded Abstracts, 627-630.

Garotta, R., Dariu, H., and Granger, P., 2000, Defining seismic velocities and density from P and S (or PS) seismic data: Presented at SEG/EAGE Summer Workshop, Boise.

Goodway, B., Chen, T., and Downton, J., 1997, Improved AVO fluid detection and lithology discrimination using Lamé petrophysical parameters; "$\lambda\rho$", "$\mu\rho$", & "λ/μ fluid stack", from P and S inversions: 67th Ann. Internat. Mtg., Soc. Expl. Geophys., Expanded Abstracts, 183-186.

Gray, D., Goodway, B., and Chen, T., 1999, Bridging the gap: using AVO to detect changes in fundamental elastic constants: 69th Ann. Internat. Mtg., Soc. Expl. Geophys., Expanded Abstracts, 852-855.

Hilterman, F., 1989, Is AVO the seismic signature of rock properties? 59th Ann. Internat. Mtg., Soc. Expl. Geophys., Expanded Abstracts, 559.

Hilterman, F., 1990, Is AVO the seismic signature of lithology? A case history of Ship Shoal-South addition: Geophysics: The Leading Edge of Exploration, **9**, 15-22.

Jin, S., 1999, Characterizing reservoir by using jointly P- and S-wave AVO analysis: 69th Ann. Internat. Mtg., Soc. Expl. Geophys., Expanded Abstracts, 687-690.

Jin, S. and Michelena, R.J., 2000, Prestack inversion of multi-component data from complex structure: Mahogany Field example, Gulf of Mexico: Presented at SEG/EAGE Summer Workshop, Boise.

Jin, S., Cambois, G., and Vuillermoz, C., 2000, Shear-wave velocity and density estimation from PS-wave AVO analysis: application to an OBS dataset from the North Sea: Geophysics, **65**, 1446-1454.

Kelly, M.C. and Ford, D., 2000a, The interpretation of P-P AVO cross-plot: 69th Ann. Internat. Mtg., Soc. Expl. Geophys., Expanded Abstracts, 214-217.

Kelly, M.C. and Ford, D., 2000b, P-S AVO attributes and cross-plotting: 69th Ann. Internat. Mtg., Soc. Expl. Geophys., Expanded Abstracts, 218-221.

Kelly, M.C., Skidmore, C.M., and Cotton, R., 2000, P-P and P-S angle stack inversion: 69th Ann. Internat. Mtg., Soc. Expl. Geophys., Expanded Abstracts, 222-223.

Kim, K.Y., Wrolstad, K.H., and Aminzadeh, F., 1993, Effects of transverse isotropy on P-wave AVO for gas sands: Geophysics, **58**, 883-888.

Knott, C.G., 1899, Reflexion and refraction of elastic waves with seismological applications: Phil. Mag., **48**, 64-97.

Koefoed, O., 1955, On the effect of Poisson's ratios of rock strata on the reflection coefficients of plane waves: Geophys. Prosp., **3**, 381-387.

Larsen, J.A., Margrave, G.F., and Lu, H., 1999, AVO analysis by simultaneous P-P and P-S weighted stacking applied to 3C-3D seismic data: 69th Ann. Internat. Mtg., Soc. Expl. Geophys., Expanded Abstracts, 721-723.

Mahob, P.N., Castagna, J.P., and Young, R.A., 1999, AVO inversion of a Gulf of Mexico bright spot-a case study: Geophysics, **64**, 1480-1491.
Malkin, A., Zakhem, U.I., and Canning A., 1999, Amplitude inversion of reflectivity type AVO attributes: 69th Ann. Internat. Mtg., Soc. Expl. Geophys., Expanded Abstracts, 812-815.
Mallick, S. and Frazer, L.N., 1991, Reflection/transmission coefficients and azimuthal isotropy in marine studies: Geophys. J. Internat., **105**, 241-252.
Ostrander, W.J., 1984, Plane-wave reflection coefficients for gas sands at nonnormal angles of incidence: Geophysics, **49**, 1637-1648.
Ramos, A.C.B., Oliveira, A.S., and Tygel, M., 1999, The impact of true amplitude DMO on amplitude versus offset: 69th Ann. Internat. Mtg., Soc. Expl. Geophys., Expanded Abstracts, 832-835.
Richards, P.G. and Frasier, C.W., 1976, Scattering of elastic waves from depth-dependent inhomogeneties: Geophysics, **41**, 441-458.
Ronen, S., Goodway, B., Young, P., Ozdemir, H., and Engelmark, F., 2000, Simultaneous multi-component AVO inversion: Presented at SEG/EAGE Summer Workshop, Boise.
Ross, C.P., and Sparlin, M.A., 2000, Improved crossplot analysis using visualization techniques: The Leading Edge, **19**, 1188-1199.
Rousseeuw, P.J. and Leroy, A.M., 1987, Robust regression and outlier detection: Wiley Series in Probability and Mathematical Statistics.
Rüger, A., 1997, P-wave reflection coefficients for transversely isotropic models with vertical and horizontal axes of symmetry: Geophysics, **62**, 713-722.
Rüger, A., 1998, Variation of P-wave reflectivity with offset and azimuth in anisotropic media: Geophysics, **63**, 935-947.
Rutherford, S.R. and Williams, R.H., 1989, Amplitude-versus-offset variations in gas sands: Geophysics, **54**, 680-688.
Shuey, R.T., 1985, A simplification of the Zoeppritz equations: Geophysics, **50**, 609-614.
Smith, G.C. and Gidlow, P.M., 1987, Weighted stacking for rock property estimation and detection of gas: Geophys. Prosp., **35**, 993-1014.
Swan, H.W., 1991, Amplitude-versus-offset measurement errors in a finely layered medium: Geophysics, **56**, 41-49.
Thomsen, L., 1993, Weak anisotropic reflections, *in* Castagna, J. and Backus, M., Eds, Offset-dependent reflectivity – Theory and practice of AVO analysis: Soc. Expl. Geophys., 103-114.
Thomsen, L., 1999, Converted-wave reflection seismology over inhomogeneous, anisotropic media: Geophysics, **64**, 678-690.
Verm, R. and Hilterman, F., 1995, Lithology color-coded seismic sections: The calibration of AVO crossplotting to rock properties: The Leading Edge, **14,** 847-853.
Wang, Y., 1999, Approximations to the Zoeppritz equations and their use in AVO analysis: Geophysics, **64**, 1920-1927.
Wapenaar, K., 1999, Amplitude-variation-with-angle behavior of self-similar interfaces: Geophysics, **64**, 1928-1938.
Wapenaar, K., van Wijingaarden, A-J., van Geloven, W., and van der Leij, T., 1999, Apparent AVA effects of fine layering: Geophysics, **64**, 1939-1948.
Waters, K.H., 1981, Reflection Seismology: A tool for energy resource exploration: John Wiley & Sons, Inc.
Wright, J., 1997, The effects of transverse isotropy on reflection amplitude versus offset: Geophysics, **52**, 564-567.
Zoeppritz, K., 1919, Erdbebenwellen VIIIB, On the reflection and propagation of seismic waves: Göttinger Nachrichten, I, 66-84.

REFERENCES FOR GENERAL READING

Frasier, C.W., 1988, AVO: Usage/misusage: 58th Ann. Internat. Mtg., Soc. Expl. Geophys., Expanded Abstracts, 1356.
Gardner, G.H.F., Gardner, L. W., and Gregory, A. R., 1974, Formation velocity and density-the diagnostic basics for stratigraphic traps: Geophysics, **39**, 770-780.
Lines, L.R. and Treitel, S., 1984, Tutorial: A review of least-squares inversion and its application to geophysical problems: Geophys. Prosp., **32**, 159-186.
Stewart R.R., Zhang, Q., and Guthoff, F., 1995, Relationships among elastic-wave values (R^{pp}, R^{ps}, R^{ss}, Vp, Vs, ρ, σ, κ) CREWES Report **7**, 10, 1-9.

Ursin, B. and Tjaland, E., 1992, Information content of the elastic reflection matrix: 62nd Ann. Internat. Mtg., Soc. Expl. Geophys., Expanded Abstracts, 796-799.
Walden, A.T., 1991, Making AVO sections more robust: Geophys. Prosp., **39**, 915-942.

APPENDIX A

THE AKI-RICHARDS (1980) MATRIX REPRESENTATION OF THE KNOTT-ZOEPPRITZ EQUATIONS (FROM CASTAGNA AND BACKUS, 1993)

APPENDIX A—MATRIX REPRESENTATION OF THE KNOTT-ZOEPPRITZ EQUATIONS

Aki and Richards (1980) give the Knott-Zoeppritz equations in convenient matrix form. For completeness they are repeated here.

For an interface between two infinite elastic half-spaces, there are sixteen reflection and transmission coefficients (see Figure A-1). In the Aki and Richards notation, the coefficients are represented by two letters (e.g. $\grave{P}\acute{S}$). The first letter indicates the type of incident wave and the second letter represents the type of derived wave. The acute accent (´) indicates an upgoing wave while a downgoing wave has a grave accent (`). Thus, $\grave{P}\acute{S}$ is the downgoing P-wave to upgoing S-wave coefficient. With this notation, the scattering matrix is

$$\underline{\mathbf{Q}} = \begin{pmatrix} \grave{P}\acute{P} & \grave{S}\acute{P} & \acute{P}\acute{P} & \acute{S}\acute{P} \\ \grave{P}\acute{S} & \grave{S}\acute{S} & \acute{P}\acute{S} & \acute{S}\acute{S} \\ \grave{P}\grave{P} & \grave{S}\grave{P} & \acute{P}\grave{P} & \acute{S}\grave{P} \\ \grave{P}\grave{S} & \grave{S}\grave{S} & \acute{P}\grave{S} & \acute{S}\grave{S} \end{pmatrix} = \underline{\mathbf{P}}^{-1}\underline{\mathbf{R}} \qquad \text{(A-1)}$$

where $\underline{\mathbf{P}}$ is the matrix

$$\begin{pmatrix} -\sin\Theta_1 & -\cos\Phi_1 & \sin\Theta_2 & \cos\Phi_2 \\ \cos\Theta_1 & -\sin\Phi_1 & \cos\Theta_2 & -\sin\Phi_2 \\ 2\rho_1 V_{S1}\sin\Phi_1\cos\Theta_1 & \rho_1 V_{S1}(1-2\sin^2\Phi_1) & 2\rho_2 V_{S2}\sin\Phi_2\cos\Theta_2 & \rho_2 V_{S2}(1-2\sin^2\Phi_2) \\ -\rho_1 V_{P1}(1-2\sin^2\Phi_1) & \rho_1 V_{S1}\sin 2\Phi_1 & \rho_2 V_{P2}(1-2\sin^2\Phi_2) & -\rho_2 V_{S2}\sin 2\Phi_2 \end{pmatrix}$$

and $\underline{\mathbf{R}}$ is the matrix

$$\begin{pmatrix} \sin\Theta_1 & \cos\Phi_1 & -\sin\Theta_2 & -\cos\Phi_2 \\ \cos\Theta_1 & -\sin\Phi_1 & \cos\Theta_2 & -\sin\Phi_2 \\ 2\rho_1 V_{S1}\sin\Phi_1\cos\Theta_1 & \rho_1 V_{S1}(1-2\sin^2\Phi_1) & 2\rho_2 V_{S2}\sin\Phi_2\cos\Theta_2 & \rho_2 V_{S2}(1-2\sin^2\Phi_2) \\ \rho_1 V_{P1}(1-2\sin^2\Phi_1) & -\rho_1 V_{S1}\sin 2\Phi_1 & -\rho_2 V_{P2}(1-2\sin^2\Phi_2) & \rho_2 V_{S2}\sin 2\Phi_2 \end{pmatrix}.$$

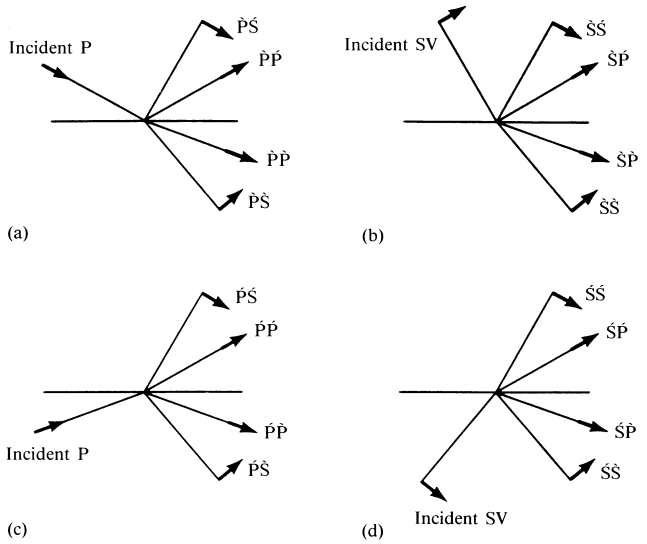

Fig. A-1. Notation for the sixteen possible reflection/transmission coefficients for P-SV waves at an interface between two different solid half-spaces. Short arrows show the directions of particle motion (from Aki and Richards, 1980).